academicJournals

Vol. 8(9), pp. 327-334, 9 March, 2013
DOI: 10.5897/IJPS11.1281
ISSN 1992-1950 © 2013 Academic Journals
http://www.academicjournals.org/IJPS

International Journal of Physical Sciences

Full Length Research Paper

Mechanical characterization of nickel plated copper heat spreaders with different catalytic activation surface treatment techniques

Victor C. H. Lim[1,2]*, Nowshad Amin[1], Foong Chee Seng[3], Ibrahim Ahmad[4] and Azman Jalar[2]

[1]Department of Electrical, Electronic and Systems Engineering, Faculty of Engineering and Built Environment, Universiti Kebangsaan Malaysia, Bangi, Selangor, Malaysia.
[2]Microelectronics Semiconductor Packaging, Institute of Micro Engineering and Nanoelectronics, Universiti Kebangsaan Malaysia, Bangi, Selangor, Malaysia.
[3]Freescale Semiconductor (M) Sdn. Bhd., Petaling Jaya, Selangor, Malaysia.
[4]Department of Electronics and Communication, College of Engineering, University Tenaga Nasional, Kajang, Selangor, Malaysia.

Accepted 5 March, 2013

This paper studied the effects of different catalytic activation processes towards intermetallic diffusion and mechanical properties on nickel plated heat spreader after high temperature storage (HTS). Heat spreader performs as medium to dissipate heat from silicon die towards heat-sink and is normally made by copper that is plated with nickel to improve wear resistance and prevent oxidation of copper. Two types of heat spreader that using galvanic initiation and thin nickel-copper electrodeposition surface treatment technique had been studied on their hardness and moduli by using Micro Tester and Nano-indenter. Besides, HTS tests were performed to investigate intermetallic diffusion between the nickel and copper layers. Young's moduli of the heat spreaders which were plated by galvanic initiation and thin nickel-copper strike electroless nickel plating catalytic activation techniques were 45 to 65 GPa and 60 to 80 GPa, respectively. The results found that thin nickel-copper electrodeposition technique gave a higher modulus for the heat spreader and this also increased the mechanical strength of heat spreader. Diffusion also took place with a very slow rate in nickel-copper layer.

Key words: Heat spreader, electroless nickel plating, galvanic initiation, thin nickel-copper electrodeposition, high temperature storage.

INTRODUCTION

Thermal is an important issue for latest semiconductor package. This is due to more energy that have been generated in high power and processing speed packages. Among these packages, flip chip ball grid array (FCBGA) is the packaging type that creates most heat during operation in high frequency application (Samson et al., 2005; Kutz, 2005). The ability for the substrate to transfer heat out from the junction is quite limited, especially for epoxy and plastic substrates which are made from low conductivity material. Therefore, a highly conductive component like the heat spreader needs to be attached onto the other side of the die to transfer heat of the junction in the opposite direction which was shown in Figure 1 (Samson et al., 2005; Bolanos, 2007; Ohadi and Qi, 2004). Heat spreader is normally made from copper because copper is a material

*Corresponding author. E-mail: viclimch@eng.ukm.my.

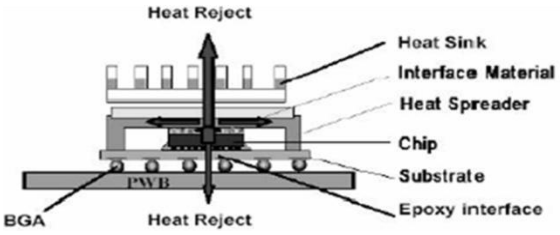

Figure 1. Schematic of thermal packaging architecture.

of high thermal conductivity (Cengel, 2006). However, copper easily oxidises with air, and copper oxide is not a ductile material (Callister, 1999). Copper oxide will affect the performance of the heat spreader. Copper oxide is also an irritant that causes health implications to human body. Therefore, nickel is plated onto the copper heat spreader to prevent copper oxidation from occurring. Although nickel is also a highly reactive element, it reacts very slowly in room temperature and ambient pressure (Callister, 1999). Due to its slow oxidation rate, nickel has been commonly used for the plating of other metals.

Advantages of electroless plated nickel over electroplated nickel include higher corrosion resistance, a very uniform thickness over the most complicated shapes, high after-plated hardness, very high hardness after a heat treatment procedure, high solderability and bondability, and control over magnetic properties (Durkin et al., 1993; Kanungo et al., 2006; Taheri, 2003). Electroless nickel plating is an autocatalytic process that does not use externally applied electric current to deposit a layer of nickel alloy with the reducing agent (Taheri, 2003; Chen et al., 2003). An electroless deposition process uses only one electrode without external source of electrical current. However, the solution for the electroless process involves a reducing agent so that the electrode reaction can take place. The electrons are supplied by this reducing agent, normally hypophosphite that is dissolved in the plating solution. The deposited nickel acts as a catalyst for the continuation of the chemical reaction until the plating process is terminated by taking out the deposited part from the bath (Chen et al., 2003; Kantola, 2006; Van Den Meerakker, 1980; Watanabe and Honma, 1998). Electroless nickel plating process starts spontaneously for some material when immersed into the electroless nickel plating solution, provided that there is a chemically clean surface. For some other materials like plastics, ceramics, silver, copper and copper alloys, catalytic activation is required to initiate the chemical reduction process (Kantola, 2006; Van Den Meerakker, 1980). Prior to the process of electroless nickel plating, copper or copper alloys need to go through several cleaning and activation processes. The purpose of these processes is to clean the oxide layer and other impurities, and provide a suitable surface for chemical reduction process. The success for copper depends upon the activation process used. Some copper and copper alloys will not catalytically initiate plating in the nickel phosphorus systems without an additional activation process after normal preparation (Durkin et al., 1993; McKinnon, 2003).

Two types of nickel plated copper heat spreader were used in the assembly of flip-chip ball grid array packages. A difference in performance from the package was noticed after the assembly process. After both heat spreaders had been cross sectioned, one of the heat spreader was found to have an additional thin layer between the electroless nickel deposit layer and copper layer. The objective of this paper is to determine the intermetallic diffusion between each layer for different catalyst activation process after high temperature storage. Besides, this paper also studies the moduli and hardness test in determining mechanical properties for heat spreaders.

MATERIALS AND METHODS

Designs of heat spreaders in this project were in accordance to the 33 × 33 mm FCBGA package and the 30 × 30 mm heat sink. The area of the heat spreader was 30 × 30 mm which matched the heat sink. The heat spreaders were made from copper and plated with nickel. The copper heat spreaders were sent to two different metal finishing suppliers which used different catalytic activation processes. One of the suppliers used nickel-copper strike as catalytic activation technique while another supplier used galvanic initiation as their catalytic activation process. The heat spreaders that were plated with nickel-copper strike catalytic activation technique were named as heat spreader A, while the heat spreaders that were plated using the galvanic initiation catalytic activation technique were named as heat spreader B. The intrinsic properties of the heat spreaders were assumed to be the same but difference in catalytic activation technique before electroless plating process.

After the heat spreaders were received from suppliers, most of the heat spreaders were put into the high temperature storage (HTS) oven for the HTS test. HTS tests for heat spreaders were performed at 150°C for 24, 48, 96 and 168 h, respectively. The HTS ovens that were used in this project were HTS oven and profiler oven. Accelerated aging at high temperature was used to promote nickel-copper intermetallic growth. All the samples with same initial catalytic activation techniques were baked under different time ranges to see the growth of catalytic activation layer. After the heat spreaders were taken out from the HTS oven, some heat spreaders were cross-sectioned using the normal metallographic manner. Cross sections of heat spreaders were prepared by using grinding and cross section machine, extra precautions were taken not to smear the thin metal layers. Proper processing steps were required to ensure quality encapsulation of the samples. In addition, the deformation of the thin metal layers due to the polishing process had to be minimized. After the samples had been cross-sectioned, optical images of each sample were taken by high power microscope under x1000 magnification. Finally the thickness of each layer had been taken using camera microscope and was measured by measurement software.

Both types of heat spreaders after HTS test were sent for mechanical properties tests. These tests provided information about the effect of different electroless nickel plating catalytic activation techniques towards mechanical behaviors of the heat spreaders. Young's Modulus of the heat spreaders was determined by the three points bending test using Instron Micro Tester. Specimens

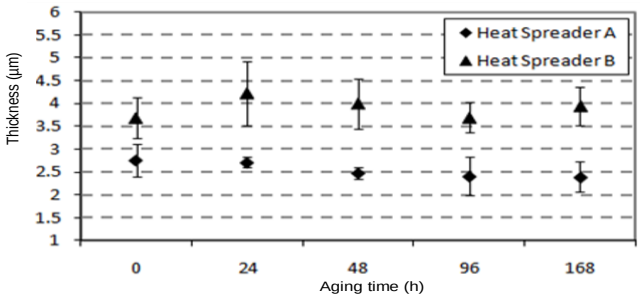

Figure 2. Nickel-phosphorus thicknesses of heat spreader A and B under different time conditions with 95% confidence interval for the mean.

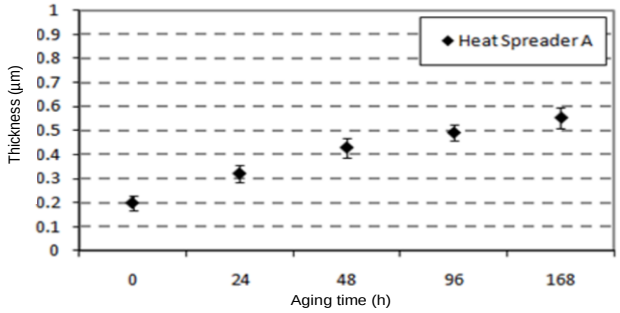

Figure 3. Nickel-copper thicknesses of heat spreader A under different time conditions with 95% confidence interval for the mean.

were supported as a simple beam, with the compressive load being applied at midpoint, and maximum stress and strain were calculated.

Apart from that, the hardness and reduced modulus of heat spreaders were determined by nano indentation test using nano indenter. For indentation, a prescribed load was applied to an indenter in contact with a specimen. The probe was forced into the surface at a selected rate and to a selected maximum force. The depth of penetration was measured when the load was applied. The area of contact at full load was determined by the depth of the impression and the known angle or radius of the indenter. A force-displacement curve had been obtained during indentation provided indications of the sample material's mechanical and physical properties.

RESULTS AND DISCUSSION

Intermetallic diffusion after high temperature storage

The purpose of this study is to evaluate intermetallic diffusions between each layer of heat spreader under HTS thermal aging conditions. Intermetallic diffusions for each heat spreaders layer under HTS conditions were investigated in this section using normal metallographic cross section manner. Figure 2 shows the nickel-phosphorus thicknesses for heat spreader A and B while Figure 3 shows the nickel-copper thicknesses for heat spreader A after HTS thermal aging. Figure 2 illustrates the electroless nickel plating layer thickness of heat spreader A is slightly reduced from the initial (*T0*) thickness of 2.8 to 2.4 µm after 168 aging h. Meanwhile, Figure 3 illustrates the nickel-copper electrodeposition layer thickness of heat spreader A increased from the initial thickness of 0.2 to 0.6 µm after 160 h aging time. Both results demonstrated that intermetallic diffusion took place on the nickel-copper layer towards the other layers. The diffusion of nickel-copper electrodeposition layer actually occurred in two directions; that is, in the direction of the nickel-phosphorus and copper layers. The diffusion coefficient, *D*, is the rate at which atoms diffuse. The equation of the diffusion coefficient is as follows:

$$D = D_0 \exp(-Q_d/RT) \qquad [m^2/s] \qquad (1)$$

Where D_0 is the temperature-independent pre-exponential, Q_d is the activation energy for diffusion, R is the gas constant, 8.31 J/molK and T is the absolute temperature. The nickel-copper metal diffusion rate is slow because of its low temperature-independent pre-exponential (D_0 = 2.7 × 10^{-5} m^2/s) and high activation energy (Q_d = 256 K) compared with other metals (Callister, 1999; Wulff et al., 2004).

Figure 2 illustrates the thickness of nickel-phosphorus layer for heat spreader B are ranging between of 3.6 and 4.3 µm. The results did not indicate any trends in terms of the thickness of the nickel-phosphorus layer. Under all aging conditions, it was found that heat spreader B did not have any diffusion layers forming between the electroless nickel plating layer and the copper layer. The deposited atoms are arranged neatly onto the copper surface during the electroless nickel plating deposition process. There is not enough vacancy for copper atoms to diffuse into the electroless nickel plating layer (Durkin et al., 1993; McKinnon, 2003). Therefore, electroless nickel plating layer provides strong resistance against wear and tear, and is able to act as anti-corrosion material for today's industry.

For the nickel-copper electrodeposition layer in heat spreader A, the nickel and copper atoms created some vacancies during deposition onto the surface of copper. This made the copper and nickel atoms diffuse easily inside the nickel-copper electrodeposition layer. Strike plating method was used in combination with the plating of different metals where the deposits of the strike method become the foundation for subsequent plating processes. Strike method normally uses a high current density and a bath with a low ion concentration (Durkin et al., 1993; Singh et al., 2006; Dini, 1993; Marquis et al., 2006). However, this plating process is extremely slow and takes time. In order to shorten the strike time, manufacturer normally increases the bath ion concentration. Nevertheless, if the deposition rate is too high, poor adhesion and plating quality will occur (McKinnon, 2003; Dini, 1993; Fritz et al., 2001). This is because the deposits do not arrange orderly on the

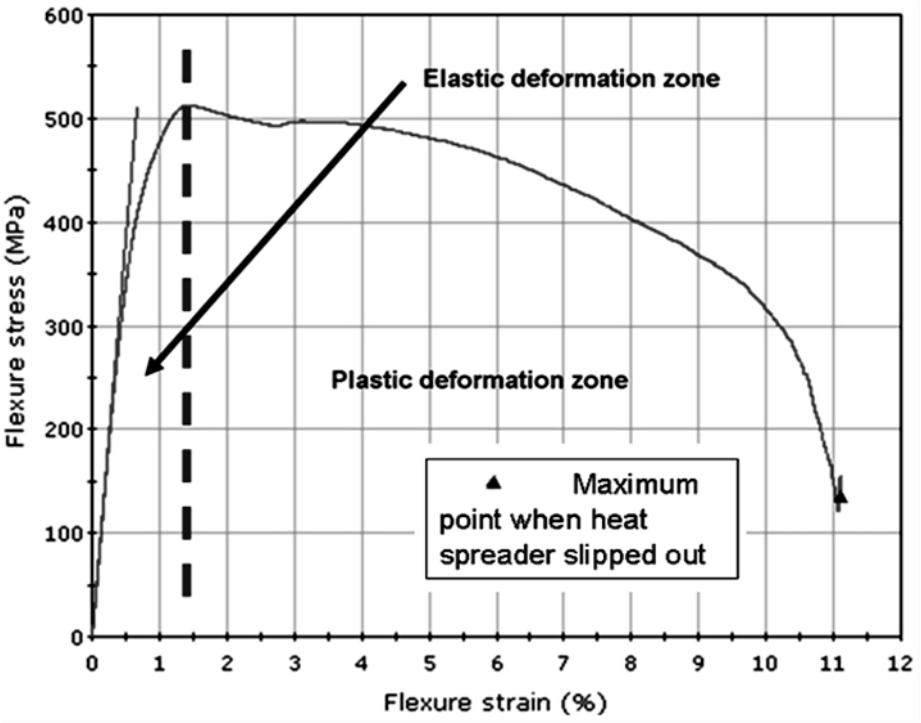

Figure 4. Graph of 3-points bending flexure stress against flexure strain for heat spreader.

substrate and creates vacancies between the deposits. In the case of heat spreader A, increasing the strike rate did not affect the plating quality. Instead, the vacancies between the deposited atoms help to promote intermetallic diffusion of the nickel-copper layers.

Effect of catalytic activation technique towards mechanical properties

Characterization of mechanical properties in this study involved two parts, namely 3-points bending test and nano-indentation test. 3-point bending test provided the Young's Modulus information on heat spreaders while nano-indentation provided hardness and reduced modulus parameters for the heat spreaders. Both of these parameters prove to be useful information in identifying the mechanical properties of heat spreaders which were produced using different catalytic activation processes.

3-point bending test is a flexural stress versus strain test that is able to calculate the modulus of elasticity (Young's modulus). 3-point bending test was chosen as the mechanical tensile test instead of the tension test because the probability of heat spreader being bent in the package during operation is higher than being pulled. This phenomenon happens when the package faces warpage effect due to coefficient of thermal expansion (CTE) mismatch inside the package (Kutz, 2005). The output of this test is recorded on a strip chart as load versus elongation, which is dependent on the specimen's size. In order to calculate modulus in an easier way, load and elongation are normalized to the flexure stress and flexure strain to minimize the geometrical factors. Flexure stress (σ) is equal to the load force (F) divided by original cross-section area (A_0) which is shows in Equation 2. Flexure strain (ε) is equal to deformation elongation (Δl) divided by original length (l_0) which is shows in Equation 3.

$$\sigma = F / A_0 \quad [\text{Pa}] \tag{2}$$

$$\varepsilon = \Delta l / l_0 \tag{3}$$

Figure 4 shows the graph of flexure stress against flexure strain after normalisation. From the graph, the mechanical behaviour of the heat spreader in the bending test can be divided into two parts which were elastic deformation zone and plastic deformation zone. Young's modulus was calculated by the gradient of the elastic deformation zone, which is flexure stress divided by flexure strain. The mechanical behaviour of the heat spreader was the same as metal and metal alloys by having a high Young's modulus and wide plastic deformation zone (Callister, 1999).

During the test, it was found that the heat spreaders were not broken and the test ended when the heat spreaders started slipping out of the test platform. This is

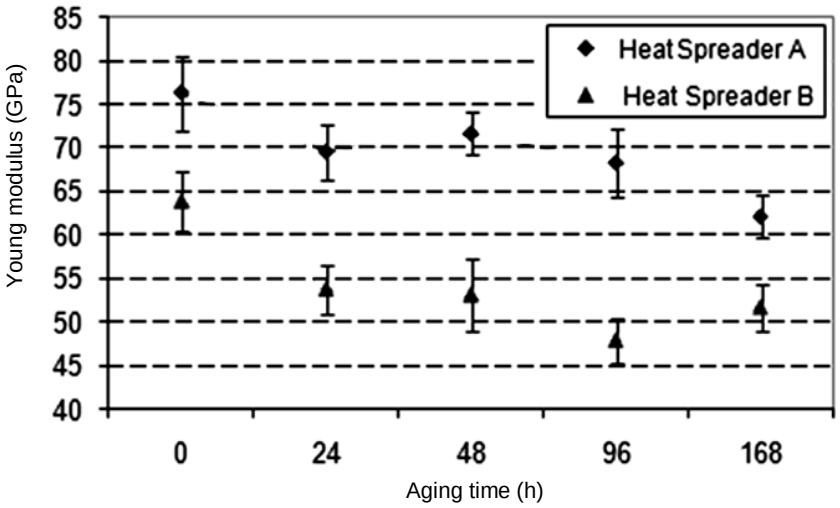

Figure 5. Young's moduli of heat spreader A and B under different time conditions with 95% confidence interval for the mean.

because heat spreader was made by copper, which is a very ductile material that is not easily broken during the bending test. Both heat spreaders' electroless nickel plating layers were checked after the test ended. There were no peelings or cracking lines found on the electroless nickel plating layers. This means that both nickel-phosphorus layers, which were deposited by different catalytic activation processes, still maintained the ductility of the heat spreader.

Young's moduli of the heat spreaders under different HTS conditions were plotted. Figure 5 shows the Young's modulus of thin nickel-copper strike and galvanic initiation heat spreaders (heat spreader A and B). The results show the Young's moduli of the heat spreader A are in the range of 60 and 80 GPa, while Young's moduli of the heat spreader B are in the range of 45 and 65 GPa. The higher Young's modulus of heat spreader A is probably due to the nickel-copper electrodeposition layer, since nickel-copper electrodeposition layer is actually a metal alloy layer made up of a mixture of copper and nickel metals (Callister, 1999; Tench and White, 1984).

Alloys have higher Young's modulus than pure metals because impurity atoms that exist inside the solid solution customarily enforce lattice strains on the surrounding host atoms. Lattice strain field interaction between dislocation and these impurity atoms restrict any dislocative movement. A different size of atom tends to diffuse or segregate the surrounding crystal lattice and this creates a weak bonding effect. The resistance to slip is larger when impurity atoms are present because the overall lattice strain must increase if a dislocation is torn away from them. Moreover, the same lattice strain interactions exist between impurity atoms and dislocations that are in motion during plastic deformation (Callister, 1999; Tench and White, 1984; Hanke, 2001). Therefore, a higher stress is necessary initially into plastic deformation phase for solid-solution alloys.

Nano-indentation test is a mechanical property test that enables the measurement of hardness and reduced modulus of the material at specific places. This highly localised test is very suitable to characterise the properties of thin coating, and is able to perform a small indentation in nano-scale of depth displacement. The test determines the hardness and reduced modulus of the analytical models from a load-displacement data, where force, displacement and time are recorded throughout the test (Beake and Leggett, 2002; Choi and Suresh, 2003; Dong et al., 2003; Lin et al., 2004; Van Vlient et al., 2004). Figure 6 shows the load-displacement graph plotted from results that were gathered from multiple indentation tests on the surface of the heat spreader. This graph consists of two parts of load-displacement measurement, which were collected during the loading and unloading of the indenter's head.

The load was applied to Berkovich indenter while in contact with the heat spreader. When the load was applied, the maximum measured depth of penetration was used to calculate the hardness (H) of the heat spreader (Nomura et al., 2011; Oyen, 2013; Varughese et al., 2011). In Equation 4, the hardness of the heat spreader coating was derived by dividing the maximum load (P_{max}) by the projected area of contact (A_c). The area of contact at full load was determined by the depth of the impression (h_p) and the known angle or radius of the indenter. For Berkovich indenter, the value of the contact area was calculated in the Equation 5. The reduced modulus measurement of the heat spreader coating was provided by the shape of the unloading curve. The reduced modulus, E_r was calculated according the formula provided by Equation 6, where dP/dh is the

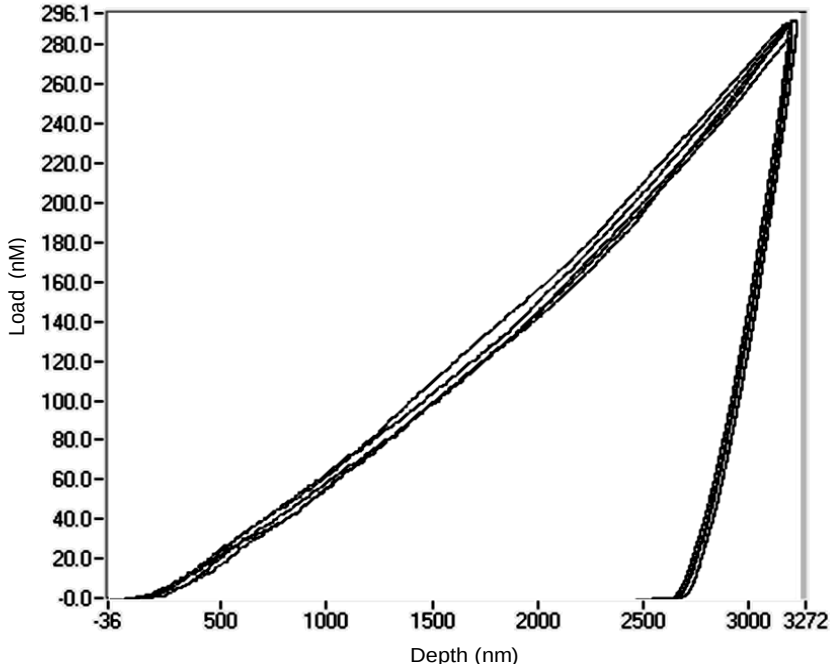

Figure 6. Graph of multiple plotting loads versus depths of heat spreader in nano-indentation test.

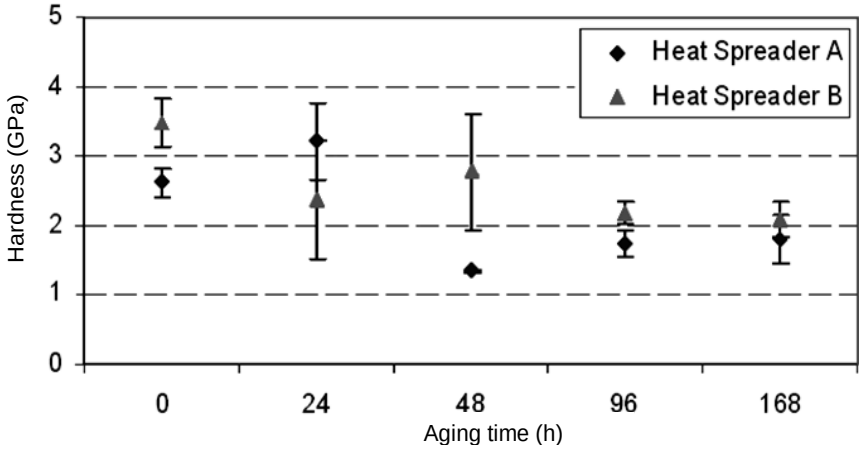

Figure 7. Hardness of heat spreader A and B under different time conditions with 95% confidence interval for the mean.

stiffness of the heat spreader coating, β is the correction index of the Berkovich indenter (Beake and Leggett, 2002; Choi and Suresh, 2003; Dong et al., 2003; Lin et al., 2004; Van Vlient et al., 2004). The following are the related equations for the nano-indentation test to determine hardness and reduced modulus:

$$H = P_{max} / A_c \quad [\text{Pa}] \quad (4)$$

$$A_c = 3(\sqrt{3})\, h_p^2 \tan^2 65.3 = 24.5\, h_p^2\ [\text{m}^2] \quad (5)$$

$$E_r = (dP / dh) \times ((\sqrt{\pi}) / 2\beta(\sqrt{A_c})) \quad [\text{Pa}] \quad (6)$$

After both results were calculated according to the respective formulas, the entire results were restructured and plotted in several graphs. Figure 7 shows the average hardness for thin nickel-copper strike and galvanic initiation heat spreaders (heat spreader A and B) under different HTS time conditions. According to the results shown in Figure 7, hardness of heat spreader A were found to be in the range of 1 and 3.5 GPa, while the

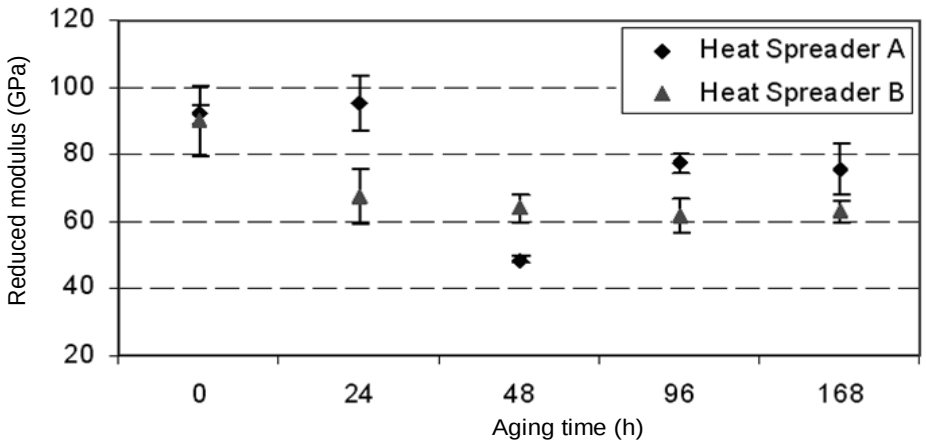

Figure 8. Reduced moduli of heat spreader A and B under different time conditions with 95% confidence interval for the mean.

hardness of heat spreader B were in the range of 2 and 3.5 GPa. Hardness of both heat spreaders are higher than the hardness of nickel, which have Vicker's hardness of 638 MPa and Brinell hardness of 700 MPa (Callister, 1999). This results show that electroless nickel plating provides a very good mechanical strength over heat spreader because electroless nickel plating layer is an alloy.

Figure 8 shows the average reduced moduli of the thin nickel-copper strike and galvanic initiation heat spreaders (heat spreader A and B). Reduced moduli of heat spreader A are between 50 and 100 GPa. Meanwhile, reduced moduli of heat spreader B are between 60 and 90 GPa. The reduced moduli of the heat spreaders are very close with reduced modulus of nickel, which is 76 GPa (Beake and Leggett, 2002).

The results of the reduced modulus can be used to determine the elasticity modulus of the sample (E_s) according to the Equation 7 with the presence of the modulus of the indenter (E_i) and the poison ratio of the sample (v_s) and the indenter (v_i) (Beake and Leggett, 2002; Choi and Suresh, 2003; Dong et al., 2003; Lin et al., 2004; Van Vlient et al., 2004).

$$1 / E_r = ((1-v_s^2) / E_s) + ((1-v_i^2) / E_i) \quad (7)$$

From the hardness and reduced modulus results that were shown by the related figures, it can be concluded that the hardness and reduced modulus of heat spreader A is slightly higher than heat spreader B. The results show a different trend compared with the Young's modulus results for the bending test because both experiments were performed under different dimensions. The bending test was performed onto the *x-y* plane of the heat spreaders while the indentation test was just performed *in-situ* onto one point of the surface of the heat spreaders.

When the heat spreaders were bent in the bending test, the whole nickel-copper deposition layer was bent together with other layers and this created significant differences in terms of results. For indentation test, electroless nickel plating layer was first indented, followed by the nickel-copper layer and lastly, the copper layer. The results were highly dependent on the hardness and the reduced modulus of the electroless nickel plating layer because this layer is thicker compared to the nickel-copper layer. Therefore, the difference of the results was not very significant for nano-indentation test.

Young's modulus, hardness and reduced modulus results showed a decrease with the increase of HTS thermal aging time. Both mechanical properties for heat spreaders with different catalytic activation processes also decreased after thermal stress was applied onto these heat spreaders. These behaviours may be due to the mechanisms of thermal stress-induced vacancy diffusion and grain boundary diffusion. These diffusions reduced the mechanical strength of the heat spreader (Callister, 1999; Wulff et al., 2004; Razeghi, 2002; Tummala, 2001). As a result, both moduli and hardnesses of the heat spreader decreased.

Conclusion

The HTS and mechanical properties of the different catalytic activation techniques were studied and compared. This study shows that under HTS condition, diffusion took place between the Ni-Cu electrodeposition layer and neighbouring layers. Young's moduli of thin nickel-copper strike and galvanic initiation techniques were 60 to 80 GPa and 45 to 65 GPa, respectively. Consequently, thin nickel-copper strike technique provided a higher mechanical strength in bending test. Differences on the heat spreaders' hardness and reduced

moduli were not significant for both catalytic activation techniques. Besides, mechanical strengths of the heat spreaders for both catalytic activation techniques decreased when thermal aging time increased.

ACKNOWLEDGMENTS

This study was supported by the Malaysia Government and Universiti Kebangsaan Malaysia, under the IRPA grant of 03-01-01-0088-PR0075/09-08 and Science Fund 03-01-02-SF0495. Special thanks also go to Freescale Semiconductor (M) Sdn. Bhd. for its assistance in providing experimental facilities.

REFERENCES

Beake BD, Leggett GJ (2002). Nanoindentation and nanoscratch testing of uniaxially and biaxially drawn poly(ethylene terephthalate) film. Polymer 43:319-327.

Bolanos MA (2007). Packaging technology trends “applied research opportunities”. USA: Texas Instruments. pp. 27-29.

Callister WD Jr (1999). Materials science and engineering: an introduction. 5th ed. USA: John Wiley & Sons, Inc. pp. 92-240.

Cengel YA (2006). Heat and Mass Transfer: A Practical Approach. 3rd ed. USA: MacGraw-Hill. pp. 844-846.

Chen WP, Lu SG, Chan HLW (2003). Influence of electroless nickel plating on I/V characteristics and its implications for reliability in ZnO-based ceramic varistors. Mater. Sci. Eng. B 99:70-73.

Choi Y, Suresh S (2003). Nanoindentation of patterned metal lines on a Si substrate. Scr. Mater. 48:249-254.

Dini JW (1993). Electrodeposition: the material science of coating and substrates. USA: Noyes Publications. pp. 46-89.

Dong S, Beake BD, Parkinson R, Xu B, Hu Z, Bell T (2003). Determination of hardness and Young’s modulus of brush plated nano-Al2O3/Ni composite coating by nanoindentation testing. Surf Eng. 19(3):195-199.

Durkin B, Barnstead M, Morcos B (1993). Basic substrate strategies and approaches for electroless nickel. USA: MacDermid, Inc. p. 1.

Fritz T, Mokwa W, Schnakenberg U (2001). Material characterisation of electroplated nickel structures for microsystem technology. Electrochim. Acta 47:55-60.

Hanke LD (2001). Handbook of analytical methods for materials. UK: Mater. Evaluation Eng. Inc. pp. 27-28.

Kantola K (2006). Modelling, estimation and control of Electroless nickel plating process of printed circuit board manufacturing. Helsinki University of Technology, Finland. pp. 3-6.

Kanungo J, Pramanik C, Bandopadhyay S, Gangopadhyay U, Das L, Saha H, Gettens RTT (2006). Improved contacts on a porous silicon layer by electroless nickel plating and copper thickening. Semicond. Sci. Technol. 21:964-970.

Kutz M (2005). Mechanical Engineers’ Handbook. 3rd ed. USA: John Wiley & Sons, Inc. pp. 257-299.

Lin JF, Wei PJ, Pan JC, Ai CF (2004). Effect of nitrogen content at coating film and film thickness on nanohardness and Young’s modulus of hydrogenated carbon films. Diam. Relat. Mater. 13:42-53.

Marquis EA, Talin AA, Kelly JJ, Goods SH, Michael JR (2006). Effect of current density on the structure of Ni and Ni-Mn electrodeposits. J. Appl. Electrochem. 36:669-676.

McKinnon HW (2003). Nickel Plating: Industry Practices Control Technology and Environmental Management. USA: EPA United States Environmental Protection Agency. pp. 2-11.

Nomura K, Chen YC, Kalia RK, Nakano A, Vashishtaa P (2011). Defect migration and recombination in nanoindentation of silica glass. Appl. Phys. Lett. 99:111906.

Ohadi M, Qi J (2004). Thermal management of harsh-environment electronics. 20th IEEE SEMI-THERM Symposium, pp. 231-240.

Oyen ML (2013). Nanoindentation of Biological and Biomimetic Materials. Exp. Tech. 37:73-87.

Razeghi M (2002). Fundamentals of solid state engineering. USA: Kluwer Academic Publisher. pp. 1-40.

Samson EC, Machiroutu SV, Chang JY, Santos I, Hermerding J, Dani A, Prasher R, Song DW (2005). Interface Material Selection and a Thermal Management Technique in Second-Generation Platforms Built on Intel Centrino Mobile Technology. Intl. Technol. J. 9(1):75-86.

Singh S, Ghosh SK, Basu S, Gupta M, Mishra P, Groverb AK (2006). Structural and Magnetic Study of an Electrodeposited Ni/Cu Thin Film by Neutron Reflectometry. Electrochem. Solid-State Lett. 9(3):J5-8.

Taheri R (2003). Evaluation of Electroless Nickel-Phosphorus (EN) Coatings. PhD dissertation, University of Saskatchewan, Canada. pp. 4-10.

Tench D, White J (1984). Enhanced tensile strength for electrodeposited nickel-copper multilayer composites. Metallurg. Trans. A 15(A):2039-2040.

Tummala RR (2001). Fundamentals of Microsystems packaging. Singapore: McGraw-Hill. pp. 212-263.

Van Den Meerakker JEAM (1980). On the mechanism of electroless plating II: one mechanism for different reductants. J. Appl. Electrochem. 11:395-400.

Van Vlient KJ, Prchlik L, Smith JF (2004). Direct measurement of indentation frame compliance. J. Mater. Res. 19(1):325-31.

Varughese S, Kiran MSRN, Solanko KA, Bond AD, Ramamurty U, Desiraju GR (2011). Interaction anisotropy and shear instability of aspirin polymorphs established by nanoindentation. Chem. Sci. 2:2236-2242.

Watanabe H, Honma H (1998). Direct Electroless Nickel Plating on Copper Circuits Using DMAB as a Second Reducing Agent. IEMT/IMC Proceedings. pp. 149-153.

Wulff F, Breach C, Stephan D, Saraswati, Dittmer K (2004). Characterization of intermetallic growth in copper and gold ball bonds on aluminum metallization. In: Proc. 6th EPTC Singapore. pp.348-353.